An infrared study of the NGC 7538 region

M. W. Werner, E. E. Becklin,★ I. Gatley, K. Matthews and G. Neugebauer *Division of Physics, Mathematics and Astronomy, California Institute of Technology, Pasadena, California, USA and Hale Observatories, California Institute of Technology, Carnegie Institution of Washington*

C. G. Wynn-Williams★ *Mullard Radio Astronomy Observatory, University of Cambridge, England*

Summary. Infrared observations of the NGC 7538 region at wavelengths from $1\,\mu m$ to $1\,mm$ are presented and analysed with the aim of understanding both the large-scale structure of this region of current star formation and the properties of the individual compact objects within it. At far-infrared wavelengths ($25-130\,\mu m$), emission is seen from the visible H II region, from the vicinity of the previously known maser sources and dust-embedded compact H II regions, and from a new region called NGC 7538(E). Coincident with NGC 7538(E) are a point-like $1-25\,\mu m$ infrared source, NGC 7538-IRS9, which probably provides the power for the far-infrared emission, and an extended source of $2.2\,\mu m$ emission which appears to be an infrared reflection nebula. NGC 7538-IRS9 strongly resembles the compact H II region NGC 7538-IRS1 in its infrared properties but shows no radio continuum emission. The compact H II regions, the maser sources and IRS9 are located within a dense molecular cloud at the edge of the optical H II region. This cloud, which has $M \sim 9 \times 10^3 M_\odot$, is detected in emission at $1\,mm$. The NGC 7538 region appears to contain examples of different stages in the formation of massive stars; it is suggested that the centre of star formation is moving systematically to the south-east in this region.

1 Introduction

NGC 7538 is a visible H II region in the Perseus spiral arm with a diameter of some 5 arcmin on the Palomar Sky Survey print (Plate 1). A number of phenomena have been observed near this optical nebula which suggest that the NGC 7538 region is a site of very recent star formation. In a 15-arcsec diameter region about 2 arcmin south-east of the centre of the

★ Present address: Institute for Astronomy, University of Hawaii, Honolulu, Hawaii, USA.

visible nebula are found three very compact H II regions (Martin 1973), not associated with any bright nebulosity (see Plate 1). These regions, called NGC 7538-IRS1, IRS2 and IRS3, are strong sources of 1–20 μm infrared emission (Wynn-Williams, Becklin & Neugebauer 1974a, henceforth WBN), and one of them, NGC 7538-IRS1,[*] has infrared properties similar to those of pre-main-sequence objects like W3-IRS5 and the Becklin–Neugebauer source in Orion. Maser emission from OH and H_2O has been found within a few arcsec of NGC 7538-IRS1; there is also a second region of OH and H_2O maser emission, called NGC 7538(S)-OH, about 80 arcsec south of IRS1 (Wynn-Williams, Werner & Wilson 1974b; Genzel & Downes 1977). The distance to NGC 7538 has been estimated to be 3.5 kpc (Israel, Habing & de Jong 1973); this distance will be adopted throughout this paper.

In this paper we present the results of observations of the NGC 7538 region at wavelengths from 1 μm to 1 mm. The region has been mapped in the far-infrared (25–130 μm) and at 1 mm. At these wavelengths, radiation has been detected from the optical H II region, from the IRS1/IRS2/IRS3 cluster, from the vicinity of the NGC 7538(S)-OH source, and from a previously unsuspected source of infrared emission, NGC 7538(E), about 2 arcmin south-east of NGC 7538-IRS1. Near-infrared (1–25 μm) observations of this new source are described in this paper, as also are the results of 2-μm spectrophotometry of NGC 7538-IRS1 and IRS2, and of a search for 2–20 μm infrared emission associated with NGC 7538(S)-OH.

2 Observations

2.1 AIRBORNE OBSERVATIONS, 25–130 μm

The 25–130 μm observations reported here were made at an altitude of 12.3 km with the 0.9-m telescope of the Kuiper Airborne Observatory (Cameron, Bader & Mobley 1971). The instrumentation, observing techniques, and data reduction are discussed in detail by Gatley *et al.* (1977). Briefly, the experiment measures the flux from the same ~1 arcmin field of view simultaneously in well-defined bands at three wavelengths, namely 30 μm ($\Delta\lambda = 10 \mu$m), 50 μm ($\Delta\lambda = 25 \mu$m) and 100 μm ($\Delta\lambda = 45 \mu$m). Guiding of the telescope is achieved by optical viewing of stars in the focal plane through a dichroic mirror; the resulting positional accuracy is ± 15 arcsec. Maps covering a region approximately 5 arcmin in extent around NGC 7538-IRS1 were constructed by sampling a grid with 30 arcsec spacing between adjacent points. The signal and reference beams were spaced by 4 arcmin. The beam profiles were mapped on Saturn, the diameter of which was 17 arcsec at the time of observation. The beams were approximately Gaussian in shape, and the full width at half maximum of the beam was 40 arcsec at 30 and 50 μm, and 55 arcsec at 100 μm. Flux calibration was achieved by observations of Jupiter, for which the far-infrared energy distribution is assumed to be given by a model based on measurements from *Pioneer 10* (Ingersoll *et al.* 1976). The measured beam profile has been integrated over the planet disk to calculate the flux reaching the detector at each wavelength.

2.2 GROUND-BASED OBSERVATIONS, 1 mm

The 1-mm observations were made using the Hale 5-m telescope during twilight hours. A composite bolometer was used as the detector, the spectral bandwidth was 0.7–1.5 mm, and the angular diameter of the beam was 55 arcsec. The instrumentation and calibration

---

[*] The designations NGC 7538-IRS1, IRS2, etc, are used to refer to compact infrared sources seen in the 1–25 μm range, while the designations NGC 7538(N), etc, are used for the regions seen at the long (25–130 μm) wavelengths where the spatial resolution is lower.
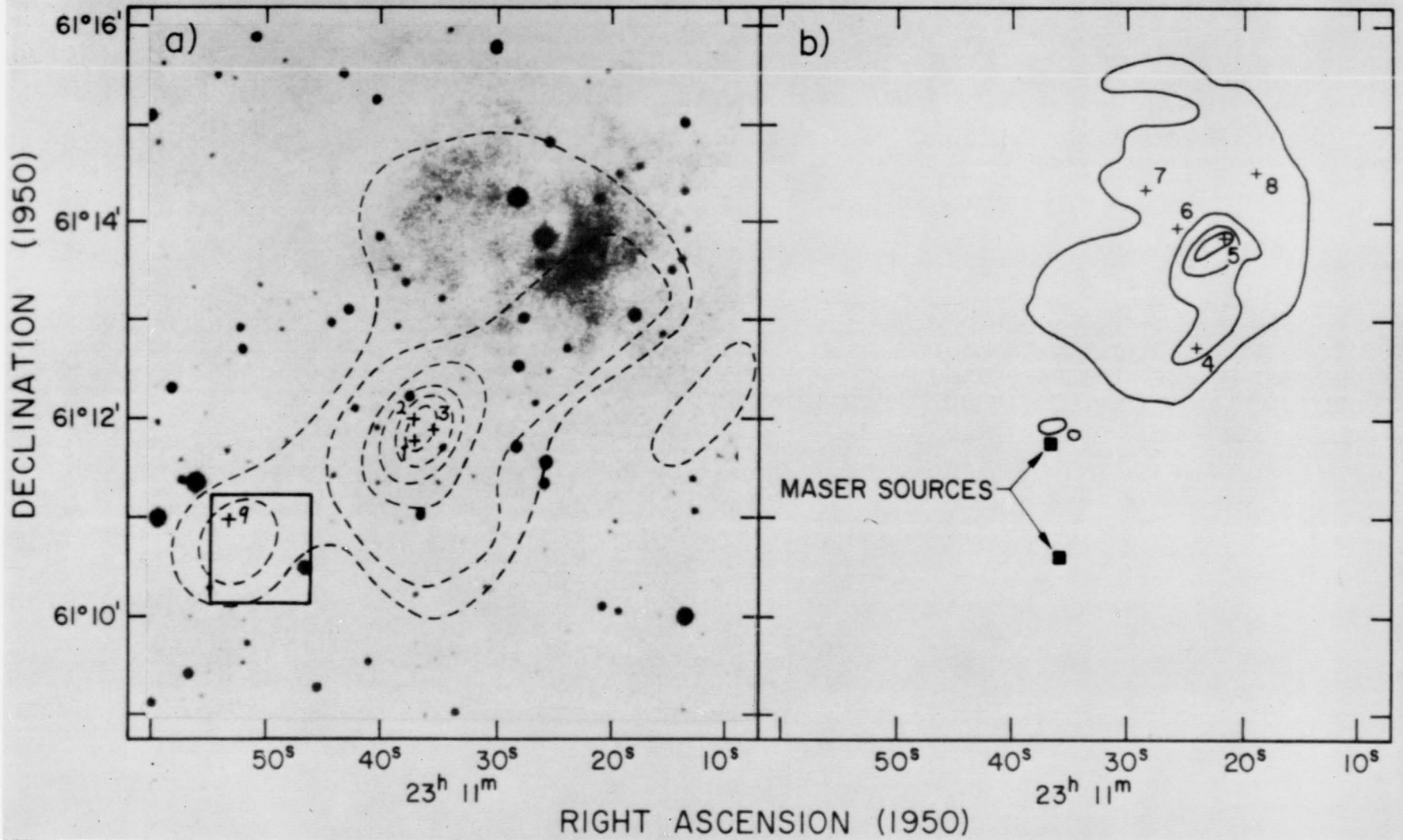
Plate 1. (a) Reproduction of the blue Sky Survey print of NGC 7538, showing the positions of the cluster of infrared sources IRS1/IRS2/IRS3 and of the newly discovered compact source IRS9. The rectangle surrounding IRS9 corresponds to the area mapped in Fig. 4. The dashed contours represent the 100μm emission as shown in Fig. 1(c). (b) The 5-GHz thermal radio emission from the NGC 7538 region adapted from Israel (1977) and Martin (1973). The northern and southern maser positions are taken from Genzel & Downes (1977). The small crosses show the positions of the 2.2-μm sources IRS4-8 found by WBN.

procedures have been fully described by Elias *et al.* (1978). The map of the NGC 7538 region was made by making measurements on a 1 arcmin grid. The absolute positional accuracy of the map is about 5 arcsec.

2.3 GROUND-BASED OBSERVATIONS, 1–25 μm

Most of the ground-based observations were carried out on the Hale 5-m telescope. An $f/16$ photometer with an InSb detector was used to scan an area about 3 arcmin in diameter around NGC 7538(N) at 2.2 μm with a resolution of 15 arcsec; a 1 arcmin region around NGC 7538(E) was scanned at 2.2 μm with this system at an angular resolution of 5 arcsec. The variation of [1.65]–[2.2] μm colour within the NGC 7538(E) region was studied on the 5-m telescope by making photometric measurements at a number of locations using a system which permitted simultaneous observations at the two wavelengths of the same 5 arcsec field of view. Two-micron spectrophotometry was performed at a few selected locations with a variable filter wheel at a spectral resolution $\lambda/\Delta\lambda \simeq 75$; the field of view for these observations was 5 arcsec. Photometry of NGC 7538-IRS9 from 3.4–12.5 μm was carried out on the Mount Wilson 1.5-m telescope using an $f/60$ chopping secondary and a germanium bolometer detection system with a 9 arcsec field of view; this system was also used at 10 μm to scan the area around NGC 7538-IRS9. A search for 10-μm emission from the NGC 7538(S) region was made with an $f/72$ photometer on the 5-m telescope, using a germanium bolometer detection system with a 4.5 arcsec field of view. This system was also used with a 1 × 4 arcsec slit to scan NGC 7538-IRS1 and IRS9 to obtain limits on their angular sizes. Finally, the NGC 7538(E), 7538(N) and 7538(S) regions were scanned at 20 μm with a 6-arcsec beam on the 2.2-m telescope at Mauna Kea, Hawaii, using the system described by Dyck & Simon (1977); photometry of IRS9 and IRS1 at 20 and 25 μm was also carried out with this system.

2.4 RADIO OBSERVATIONS

A search was made at 15 GHz for emission from NGC 7538-IRS9, using the Cambridge 5-km telescope (Ryle 1972). At this frequency the telescope has a beamwidth of 0.6 arcsec and an rms noise level of 3 mJy per beam area, or 40 K.

3 Results

3.1 FAR-INFRARED AND 1 mm MAPPING

The maps of the NGC 7538 region at 30, 50 and 100 μm (Fig. 1(a)–(c)) show three main peaks of emission. The north-westerly of these coincides approximately with the visible H II region (Plate 1), while the bright central peak, called NGC 7538(N), coincides with the previously known cluster of infrared sources IRS1/IRS2/IRS3 and their associated compact H II regions. The south-eastern feature, called NGC 7538(E), was discovered in the present series of observations on the Kuiper Airborne Observatory (Thronson *et al.* 1975); as will be described below in Sections 3.2 and 3.3, it is now known to coincide with a strong 1–25-μm point source called NGC 7538-IRS9, plus a region of extended 2.2-μm emission. On the 100-μm map an extension, NGC 7538(S), is also seen southwards towards the southern maser sources.

Thronson & Harper (1979) have also reported far-infrared mapping and photometry of the NGC 7538 region. Their results for both the spatial distribution and the total amount of

far-infrared flux are consistent with those presented here. Both NGC 7538(E) and 7538(S) appear spatially unresolved on their map with 30 arcsec resolution at an effective wavelength of 57 μm.

The 1-mm map (Fig. 1) shows a single source which peaks at NGC 7538(N) and extends toward NGC 7538(S). NGC 7538(E) lies within the outer contours of the 1-mm emission but not at a position of peak 1-mm flux. No significant 1-mm emission is seen from the vicinity of the visible H II region.

Fig. 1 shows that there are significant variations in dust temperature and opacity within the NGC 7538 region. In the vicinity of the optical H II region a temperature gradient is seen because the emission at 100 μm peaks farther south than that at 30 or 50 μm; the corresponding grain temperature (as defined in Table 1) is ~ 70 K in the centre of the H II region, decreasing to 40 K about 1.5 arcmin to the south. Emission from the vicinity of
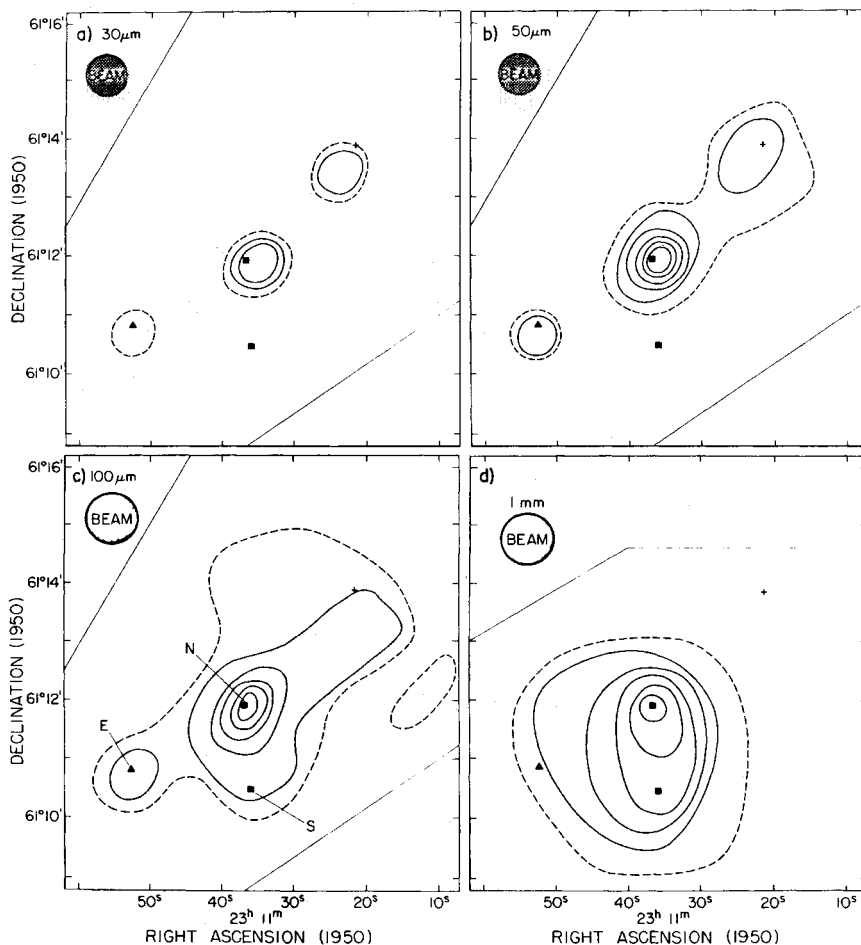
Figure 1. (a, b, c) Maps of the NGC 7538 region at 30, 50 and 100 μm made from the Kuiper Airborne Observatory. The thin straight lines show the limits of the area scanned in each case. The cross marks the position of IRS5 in the centre of the optical H II region (WBN), the two squares show the positions of the OH/H_2O masers, and the triangle is the 10-μm position of the source IRS9. The contour intervals are 1000, 1300 and 2100 Jy per beam area at 30, 50 and 100 μm corresponding to a surface brightness of 2.4, 3.1 and 2.4 $\times 10^{-16}$ W m^{-2} Hz^{-1} sr^{-1}, respectively, for a uniform brightness source. Dashed contours are at one-half of the level of the lowest full contours; the dashed contour lies at the 3 σ level of the 30- and 100-μm data and at the 5 σ level of the 50-μm data. The regions NGC 7538(N), 7538(S) and 7538(E) observed at far-infrared wavelengths (see text) are indicated on the 100-μm map (c). (d) Map of the NGC 7538 region at 1 mm made with the Hale 5-m telescope. The contour interval is 5 Jy per beam area, corresponding to a surface brightness of 3.6 $\times 10^{-19}$ W m^{-2} Hz^{-1} sr^{-1}. The dashed contour is at one-half of the level of the lowest full contour and is at the 2.5 σ level of the data.

Table 1. Far-infrared and 1-mm photometry of NGC 7538.

Region	α_{1950}	δ_{1950}	$F_{30\mu m}$ (Jy)	$F_{50\mu m}$ (Jy)	$F_{100\mu m}$ (Jy)	F_{1mm} (Jy)	$L_{25-130\mu m}$ ($10^5 L_\odot$)	T_g (K)	τ_{1mm}	M ($M_\odot$)
	h m s	$^\circ$ $'$ $''$								
Optical H II	23 11 23	61 12 50	1000	2500	5000	—	1.0	40–70	—	-
N	23 11 36	61 11 55	2300	6700	11000	30	2.5	45	4×10^{-3}	2000
S	23 11 36	61 10 30	< 500	870*	2100	20	0.2	35	4×10^{-3}	2000
E	23 11 53	61 10 40	500	1300	2700	5	0.5	40	7×10^{-4}	400

$^\star \lambda = 57 \,\mu m$, 30-arcsec diameter beam (Thronson & Harper 1979).

Explanation: The tabulated fluxes are those measured into a single beam area at the indicated positions, except for the optical H II region, where a spatial integral has been carried out. The fluxes are uncertain by ~ 30 per cent due to the calibration uncertainty; the statistical errors are smaller than this in all cases. The optical H II region was not detected at 1 mm. The grain temperatures are derived from the ratio of 50–100-μm flux, assuming that the particle emissivity varies as λ^{-1}, and the 1-mm optical depths and total (dust plus gas) masses are derived from F_{1mm} and T_g using the grain parameters given by Westbrook *et al.* (1976) and assuming a gas/dust ratio of 100 by mass.

Table 2. Positions and flux densities of compact infrared sources in the NGC 7538 region.

	IRS1	IRS9	IRS10	IRS11
Infrared position (1950)	$23^h 11^m 36^s.5 \pm 0^s.3$	$23^h 11^m 52^s.8 \pm 0^s.3$	$23^h 11^m 57^s.8 \pm 0^s.4$	$23^h 11^m 35^s.2 \pm 0^s.4$
	$61^\circ 11' 50''.5 \pm 2''$	$61^\circ 10' 59'' \pm 2''$	$61^\circ 11' 37'' \pm 3''$	$61^\circ 10' 37'' \pm 3''$
OH position (1950)	$23^h 11^m 36^s.6 \pm 0^s.4$	—	—	$23^h 11^m 36^s.1 \pm 0^s.7$
(Wynn-Williams *et al.* 1974b)	$61^\circ 11' 49'' \pm 3''$	—	—	$61^\circ 10' 29'' \pm 5''$
H_2O position (1950)	$23^h 11^m 36^s.5 \pm 0^s.3$	—	—	$23^h 11^m 36^s.3 \pm 0^s.3$
(Genzel & Downes 1977)	$61^\circ 11' 49''.5 \pm 2''$	—	—	$61^\circ 10' 29''.5 \pm 2''$
Radio position (1950)	$23^h 11^m 36^s.7 \pm 0^s.1$	—	—	—
(Harris & Scott 1976)	$61^\circ 11' 49''.6 \pm 1''$	—	—	—
$F_{1.25\mu m}$ (mJy)	—	—	35 ± 4	—
$F_{1.65\mu m}$ (mJy)	$\leqslant 10$	1.1 ± 0.1	120 ± 10	1.6 ± 0.2
$F_{2.2\mu m}$ (mJy)	190 ± 20	140 ± 20	310 ± 40	7.4 ± 0.7
$F_{3.4\mu m}$ (Jy)	—	4.2 ± 0.4	—	—
$F_{4.8\mu m}$ (Jy)	41 ± 6	28 ± 3	—	—
$F_{8.7\mu m}$ (Jy)	67 ± 9	41 ± 11	—	—
$F_{9.5\mu m}$ (Jy)	—	19 ± 3	—	—
$F_{11.2\mu m}$ (Jy)	47 ± 7	44 ± 8	—	—
$F_{12.5\mu m}$ (Jy)	149 ± 21	74 ± 13	—	—
$F_{20.0\mu m}$ (Jy)	250 ± 50	124 ± 30	—	—
$F_{25.0\mu m}$ (Jy)	640 ± 130	260 ± 50	—	—

Aperture sizes for infrared measurements: all points $\lambda < 3\,\mu m$, 5-arcsec aperture; IRS9, $3\,\mu m < \lambda < 20\,\mu m$, 9-arcsec aperture; IRS1, $3\,\mu m < \lambda < 20\,\mu m$, 7.5-arcsec aperture; IRS1 and IRS9, 6-arcsec aperture at 20 and 25 μm. Fluxes for IRS1 at 4.8, 8.7, 11.2 and 12.5 μm are from WBN.

Note: IRS11 may be unrelated to the maser sources (see text).

NGC 7538(S) is prominent only at $100\,\mu$m and 1 mm; this region is exceptionally cold ($T_g = 35$ K).

Maps of regions such as NGC 7538 at 1 mm provide a guide to the mass distribution of dust, since the emission is optically thin, and since the flux density is proportional to only the first power of the dust temperature (Westbrook *et al.* 1976). The 1-mm map (Fig. 1(d)) therefore indicates that the main concentration of dust is displaced from the centre of the optical nebula and is located instead in the vicinity of the compact infrared sources and the maser sources. The dust cloud seen at 1 mm lies at the position of peak carbon monoxide emission in the NGC 7538 region (W. J. Wilson, private communication).

Table 1 summarizes the properties of the various portions of the NGC 7538 region as inferred from the far-infrared and 1-mm observations. The observed quantities tabulated for each region of the source include the fluxes at all four wavelengths and the total far-infrared luminosity. Table 1 shows that the optical depth of dust, and thus the column density of matter, is about the same at NGC 7538(N) as at 7538(S). The total 1-mm flux within the region mapped (Fig. 1(d)) is ~ 150 Jy. If a mean grain temperature of 40 K is assumed throughout this region, the *total* mass of gas plus dust seen at 1 mm is about $9 \times 10^3 M_\odot$. The total far-infrared luminosity of the NGC 7538 region, obtained by integration of Figs 1(a)–(c), is ~ $5 \times 10^5 L_\odot$, which includes contributions from low brightness regions between the main sources listed in Table 1.

3.2 THE COMPACT SOURCE NGC 7538-IRS9

A search at $10\,\mu$m in the vicinity of the $25-130\,\mu$m source NGC 7538(E) using the 1.5-m Mount Wilson telescope led to the discovery of a single bright source with a $10\,\mu$m flux of 50 Jy. We call this source NGC 7538-IRS9. No other sources were found above a level of 10 Jy at $10\,\mu$m in a region extending 0.5 arcmin east and west and 1.5 arcmin north and south of IRS9, or at a level above 20 Jy at $20\,\mu$m in a region extending 0.5 arcmin east and west and 0.75 arcmin north and south of the object. North–south slit scans at $10\,\mu$m, made on the 5-m telescope, indicate that IRS9 is point-like with a diameter of less than 1 arcsec. The position of IRS9 (as determined with respect to nearby field stars) and the broadband infrared fluxes measured from this object in the $1.65-25\,\mu$m range are listed in Table 2.

The energy distribution of IRS9 from 1.65 to $25\,\mu$m is shown in Fig. 2; except for the $8-13\,\mu$m region, where there is a strong silicate absorption feature, and at $25\,\mu$m, where there is probably some contribution from the cooler NGC 7538(E) source, the energy distribution lies close to that of a 450 K blackbody. The bolometric luminosity of NGC 7538-IRS9 in the $1-20\,\mu$m bands is $1.2 \times 10^4 L_\odot$. Spectrophotometry in the 2.2-μm window (Fig. 3) shows a featureless spectrum with no signs of either the Bγ hydrogen emission line or the 2.3-μm CO absorption feature characteristic of late-type giant stars (Baldwin, Frogel & Persson 1973). The limit on the flux in the Bγ line is 3×10^{-16} W m^{-2}. No radio emission above a level of 10 mJy at 15 GHz is found from the position of IRS9. No visible object is seen on the Sky Survey. As seen in Fig. 2, the energy distribution of NGC 7538-IRS9 is very similar to that of NGC 7538-IRS1, although the latter appears to have a deeper silicate absorption feature.

3.3 EXTENDED EMISSION NEAR IRS9 AT 2.2 μm

Fig. 4 shows a map of the 2.2-μm emission in the vicinity of IRS9, which lies at the extreme north-eastern edge of the region mapped. The total flux density from the region mapped is ~ 400 mJy at 2.2 μm, about one-third of this being attributable to the compact source itself.

Wavelength (μm)

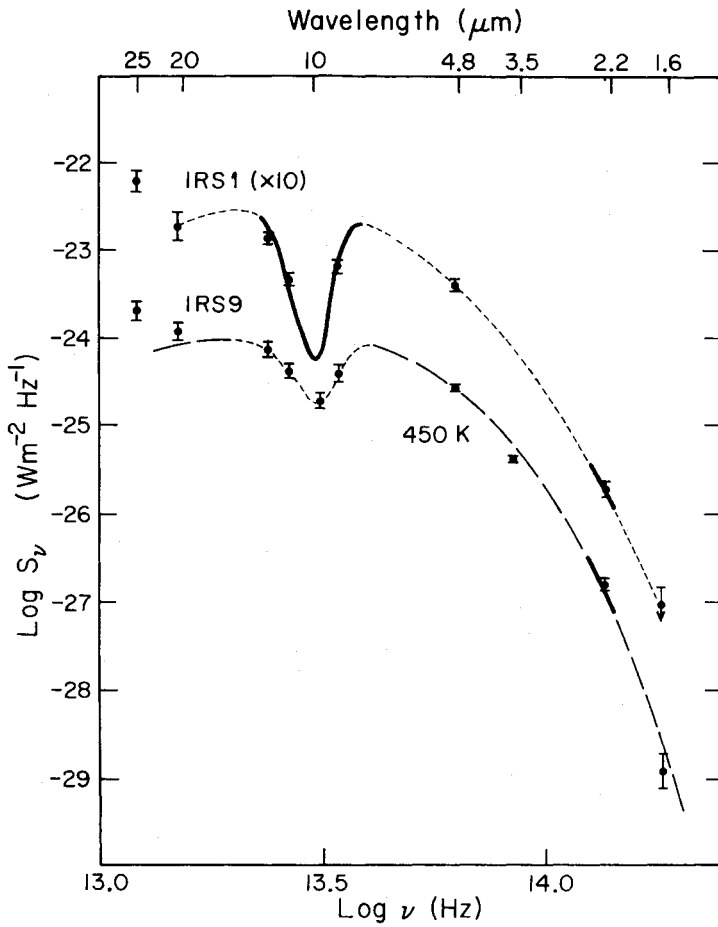Figure 2. 1.65- to 25-μm energy distributions of IRS1 and IRS9. Broadband photometry at 12.5 μm $\geqslant$ $\lambda \geqslant 3\,\mu$m of IRS1 is from WBN, while the 8–13-μm spectrophotometry of IRS1 is from Willner (1976).
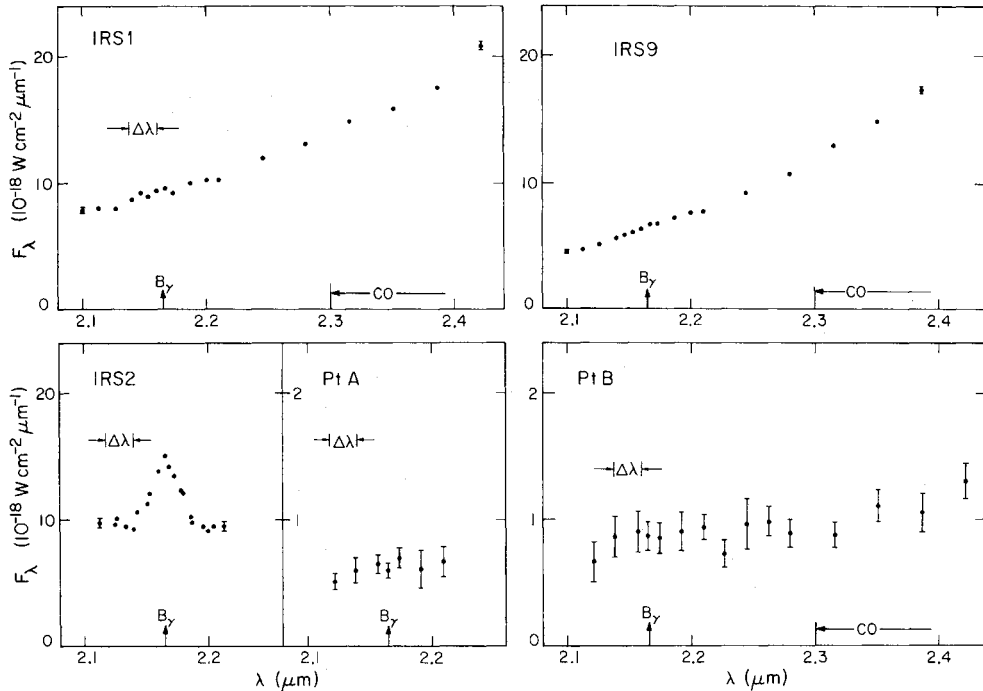
Figure 3. Spectrophotometry at five positions in the NGC 7538 region in the 2.2-μm spectral band. For IRS1, IRS2 and IRS9, typical errors are shown only on extreme points. Note that the scale changes in the case of points A and B. Each spectrum was made with a 5-arcsec diaphragm.

Two points in the region of extended emission, designated A and B in Fig. 4, have been observed spectrophotometrically at $2.2\,\mu m$ (Fig. 3). At neither point does the 2.2-μm spectrum shows any significant spectral features. The upper limit on Bγ emission from either point A or point B is $7 \times 10^{-17}\,\mathrm{W\,m^{-2}}$ within a 5 arcsec diaphragm; the corresponding equivalent width is less than $10\,\mathrm{nm}$, or one-sixth of that expected from a $10^4\,\mathrm{K}$ plasma (Wynn-Williams *et al.* 1978).
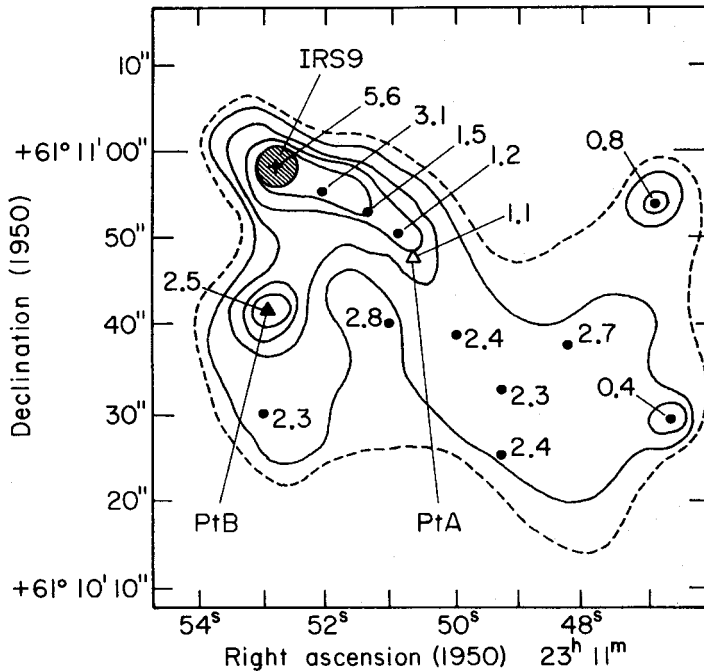

Figure 4. Map of the vicinity of NGC 7538-IRS9 at $2.2\,\mu m$. The contour interval is $7 \times 10^{-20}\,\mathrm{W\,m^{-2}\,Hz^{-1}}$ $\mathrm{sr^{-1}}$ with the dashed contour at one-half of this level. The cross denotes the position of IRS9, the open trangle that of point A, and the filled triangle that of point B. The peak of IRS9 would have 44 contours. The 2.2-μm spectra of IRS9 and of points A and B are shown in Fig. 3. The numbers refer to the $[1.65]$– $[2.2]\,\mu m$ colour indices in 5 arcsec diaphragms located at the indicated positions.

Fig. 4 also shows, superposed on the contours of 2.2-μm emission, the $[1.65]$–$[2.2]\,\mu m$ colour indices of the extended emission as determined by measuring at both wavelengths simultaneously through the same 5 arcsec diaphragm. It is seen that IRS9 is by far the reddest point and that the colour index changes extremely rapidly, by 4.5 mag in less than 20 arcsec, between IRS9 and the end of the ridge to its south-west. Apart from IRS9 and the ridge to the south-west, most of the region of extended emission has a $[1.65]$–$[2.2]\,\mu m$ colour index in the range 2.3–2.8 mag. The flux and colour information given in Fig. 4 show that the 1.65-μm flux density of IRS9 is actually *less* than that measured at any point to the south the south-west within 30 arcsec of IRS9.

The southern of the two relatively blue sources on the extreme west of Fig. 4 is a visible star (Plate 1); the isolation and colour of the northern one suggest that it may well be a reddened star unrelated to the extended source. During lower sensitivity scans of a larger region than shown in Fig. 4, a further source of 2.2-μm emission was discovered about 1 arcmin to the north-east of IRS9. Its position and flux densities are given in Table 2, where it is listed as IRS10. The colours are compatible with those of a star behind 15–20 mag of visual extinction; the source may well be unrelated to NGC 7538.

3.4 NGC 7538(S)

A search was made for infrared emission associated with the southern OH and H₂O maser sources[*], which lie in the NGC 7538(S) region about 80 arcsec south of IRS1. The OH and H₂O masers are spatially coincident within the positional uncertainties (Table 2). At 2.2 μm, a compact source, IRS11, was found about 10 arcsec from the maser position. The position and fluxes of IRS11 are given in Table 2. Additionally, faint extended emission is seen at 2.2 μm over a ~ 20 arcsec region which encompasses IRS11 and the maser sources. The average surface brightness of this 2.2-μm emission is ~ 4×10^{-20} W m^{-2} Hz^{-1} sr^{-1}, and the [1.65]–[2.2] μm colour index of the extended emission is similar to that of IRS11. No detailed information is available about the nature of IRS11 or the extended emission and their relation, if any, to the other phenomena seen in the NGC 7538 region.

A search at 10 μm of a 20 × 20 arcsec region centred on the southern OH maser position showed no emission above a level of 1 Jy in a 4.5-arcsec beam. Scans were also made at 20 μm of a region 1.2 arcmin (east–west) × 2.5 arcmin (north–south) in extent centred about 40 arcsec north and 15 arcsec east of the southern maser position; the region scanned encompasses the central portions of both NGC 7538(N) and 7538(S). No sources other than the previously known NGC 7538-IRS1/IRS2/IRS3 were found down to a level of 20 Jy in a 6-arcsec beam.

3.5 NGC 7538-IRS1 AND-IRS2

Spectrophotometry at 2.2 μm of the brightest part of the compact H II region NGC 7538-IRS2 was performed with a 5 arcsec diaphragm. The resultant profile of the hydrogen Bγ line is shown in Fig. 3. The total flux in the line is $(1.3 \pm 0.1) \times 10^{-15}$ W m^{-2}. The extinction at 2.2 μm may be estimated by comparing this infrared flux density with the 5-GHz radio emission as derived from Martin's (1973) map. The peak flux density at 5 GHz in a 5 arcsec diameter beam is 0.4 ± 0.1 Jy. Under the assumption that the infrared measurements were made at the location of maximum radio brightness, the relation between the Bγ flux and the 5-GHz radio flux density for a 10⁴ K plasma (Wynn-Williams *et al.* 1978) gives an extinction at 2.2 μm of 1.1 ± 0.3 mag; this corresponds to 11 ± 3 mag at visual wavelengths if curve 15 of van de Hulst (Johnson 1968) is used. The derived extinction is in agreement with Beetz *et al.* (1976) estimate of $A_V = 8.5$ mag based on the identification of IRS2 on an 0.92-μm photograph of the NGC 7538 region.

Spectrophotometry of NGC 7538-IRS1 (Fig. 3) shows no indication of either a Bγ emission line at 2.17 μm or a CO absorption feature at 2.3 μm. The upper limit on the Bγ flux is 3×10^{-16} W m^{-2}. By the argument used above, the fact that the 15-GHz radio flux density of IRS1 is 0.5 Jy (Harris & Scott 1976) can be used to derive a lower limit to the visual extinction to IRS1 of 30 mag, much higher than that derived for IRS2, which is only 10 arcsec away. This difference is qualitatively in agreement with the observation (Willner 1976) that IRS1 has a much deeper 10-μm silicate absorption feature than IRS2. These results indicate that much of the extinction observed to NGC 7538-IRS1 must arise within 0.2 pc of the source.

The equivalent width of the Bγ emission line is 14 ± 1 nm for NGC 7538-IRS2 and less than 5 nm for IRS1. By comparison, the equivalent width expected for Bγ from a 10⁴ K plasma is ~ 60 nm (Wynn-Williams *et al.* 1978). Therefore, it appears that the bulk of the 2-μm continuum emission from both IRS2 and, particularly, IRS1 is due to processes other

---

[*] As pointed out by Gruber & de Jager (1976), the velocity ranges at which the northern and southern OH sources in NGC 7538 were measured are interchanged in table 1 of the paper by Wynn-Williams *et al.* (1974b).

than recombination emission from the ionized gas. One possible source is emission from hot grains, as suggested by Wynn-Williams *et al.* (1978) for G333.6 − 0.2, where a similar continuum excess is seen.

The position of NGC 7538-IRS1 was redetermined relative to nearby field stars by finding the position of the peak of emission at 10 μm. As shown in Table 2, this position agrees within 2 arcsec with those determined for this object at 15 GHz, and with the OH and H_2O maser positions; it is also in agreement with the position determined at 20 μm by WBN. Slit scans of NGC 7538-IRS1 in the north–south direction show that its angular diameter at 10 μm is less than 1 arcsec.

The 2.2- and 1.65-μm flux densities for IRS1 given in Fig. 2 and Table 2 were measured through a smaller diaphragm than that used by WBN (5 instead of 7.5 arcsec); the flux densities are therefore lower. The difference is particularly significant at 1.65 μm; at this wavelength IRS1 is extremely weak and does not stand out as a clear feature above the background emission from the wings of the more extended source IRS2. The 1.65-μm flux density should therefore be regarded as an upper limit to the emission from the compact object itself.

4 Discussion: NGC 7538(E) and 7538-IRS9

4.1 THE NATURE OF NGC 7538-IRS9

Since IRS9 is a compact, luminous infrared source in a region of known recent star formation, it is natural to identify it as a protostellar object. As shown in Fig. 2, the near-infrared energy distribution of IRS9 is very similar to that of IRS1 and to that of other suspected protostellar or pre-main-sequence objects such as the Becklin–Neugebauer source in Orion, W3-IRS5 and S140-IRS (Werner, Becklin & Neugebauer 1977; Blair *et al.* 1978). Several characteristics of IRS9 which are of particular significance are:

(1) IRS9 is the only presently identified source of luminosity for NGC 7538(E). If it is in fact the only significant luminosity source in this region, the present observations fix the total luminosity of IRS9 as at least $6 \times 10^4 L_\odot$, which is the sum of the far-infrared luminosity of NGC 7538(E) plus the directly observed near-infrared luminosity of IRS9.

(2) IRS9 shows neither Bγ, radio continuum nor molecular maser emission.

(3) IRS9 is associated with a large region of extended near-infrared emission which appears to be a reflection nebulosity (see Section 4.3).

(4) Unlike many candidate infrared protostars, including NGC 7538-IRS1 (see also Westbrook *et al.* 1976), NGC 7538-IRS9 is not located at a position of peak column density as inferred from 1-mm continuum observations.

(5) IRS9 was discovered by near-infrared scans of a region identified by far-infrared observations. By contrast, most presently known objects of this type were discovered by near-infrared exploration of a known molecular emission peak, H II region or maser source.

Several of the properties of NGC 7538-IRS9 listed above will be exploited in the following section to develop a rough phenomenological model for this object.

4.2 MODELS FOR NGC 7538-IRS9

The present observations constrain the range of plausible physical models for this object. These constraints arise primarily from the suggested identification of IRS9 as the sole luminosity source for NGC 7538(E) and, to a lesser extent, from the interpretation of the region of extended 2.2-μm emission as a reflection nebulosity illuminated by IRS9.

In the first place, it can be argued that the 1–20-μm radiation received from IRS9 cannot simply be photospheric emission from a highly reddened very bright star (see, e.g. Allen & Penston 1974). If IRS9 were a highly reddened star of temperature ~ 3000 K, its bolometric luminosity would be about 50 times larger than the luminosity observed from NGC 7538(E) over all wavelengths. It would therefore be necessary that ~ 98 per cent of its visible light be lost into space. The presence of both grains hot enough to emit at 50 μm and, probably, an infrared reflection nebulosity in close proximity to IRS9 suggest, however, that it is located in a fairly dusty region. Unless some extraordinary geometric assumptions are made, therefore, it is unlikely that the required large fraction of its luminosity could escape from its vicinity without being absorbed and re-radiated in the far-infrared.

This argument shows that, regardless of the evolutionary status of IRS9, the bulk of its 1–20-μm radiation must be thermal emission from dust. Additionally, the limits on the radio emission from IRS9 show that this object produces less than 1 per cent of the ionization expected from a main sequence star with the total luminosity of NGC 7538(E). Thus the underlying energy source within IRS9 can be a main sequence star only if it is so highly dust embedded that most of the potentially ionizing photons are absorbed by dust.

If IRS9 is in fact the only source of luminosity for NGC 7538(E), the temperature of the dust radiating in the 1–20-μm waveband must be greater than the 450 K indicated by the energy distribution of IRS9, because a 450 K blackbody with the flux density shown in Fig. 2 would have a luminosity of only $1.2 \times 10^4 L_\odot$, as compared with the total measured 1–130-μm luminosity of $6 \times 10^4 L_\odot$. There must therefore be some extinction in front of IRS9 which has the effect of reducing its apparent colour temperature; this is also suggested by the presence of a 10-μm silicate absorption feature. It is reasonable to guess that the layers of dust which produce this extinction also contribute to the radiation observed at far-infrared wavelengths.

The present data can be used to estimate the temperature of the dust radiating in the near-infrared and its relationship to the dust seen at longer wavelengths. It will be assumed that the total luminosity associated with NGC 7538-IRS9 is in fact equal to $6 \times 10^4 L_\odot$; the results remain qualitatively unchanged if this is an underestimate by a factor of 2 or 3. The simplest approach is to assume two regions of dust emission — one, observed predominantly at $\lambda \leqslant 25\,\mu$m as IRS9, which is very close to the source of luminosity — and a larger region radiating principally at $\lambda \geqslant 25\,\mu$m which is observed as NGC 7538(E). The need for two fairly distinct emitting regions is suggested by the difference between the near-infrared temperature of IRS9, ~ 450 K, and the far-infrared temperature of NGC 7538(E), ~ 40 K; this idea is also supported by the break in the energy distribution of IRS9 near 25 μm (Fig. 2).

The procedure for estimating the source parameters for this model is to deredden the observed 1–20-μm energy distribution of IRS9, using the infrared extinction curve derived by Becklin *et al.* (1978), until the total luminosity of the corrected 1–20-μm energy distribution is ~ $6 \times 10^4 L_\odot$. When this is done it is found that the corrected 1-20-μm energy distribution is approximately that of a 600 K blackbody. If this object were optically thick, it would have an angular diameter of 0.06 arcsec, corresponding to a linear size of 200 AU at the distance of NGC 7538. This is consistent with the upper limit of 1 arcsec set on the diameter of IRS9 by scans at 10 μm.

The characteristic temperature of NGC 7538(E) is ~ 40 K (Table 1). If the grains have absorption efficiency varying as λ^{-1} between 5 and 50 μm, they will reach this temperature at a distance of 0.2 pc from the 600 K source with a luminosity of $6 \times 10^4 L_\odot$. The corresponding angular diameter of the far-infrared source would be (0.4 pc/3.5 kpc) $\simeq$ 20 arcsec; this is consistent with the observations by Thronson & Harper (1979) which show that NGC 7538(E) is unresolved at 57 μm with a 30-arcsec beam.

Although this model probably leads to reasonable estimates of the size and temperature of NGC 7538-IRS9, it is oversimplified because it does not explicitly consider a spatially continuous distribution of dust and also because it does not account for the region of extended 2.2-μm emission. The modifications in the model required to account for the region of extended 2.2-μm emission will be explored in the next section.

4.3 THE EXTENDED EMISSION NEAR IRS9

Fig. 3 shows that extended emission is seen at 1.65 and 2.2 μm over a 40 x 40 arcsec region to the south-west of IRS9. Unlike most known extended 2.2-μm sources, this area is not an H II region, since the absence of both radio emission (Israel *et al.* 1973) and Bγ emission (Section 3.3) indicate that not more than a few per cent of the 2.2-μm continuum from this region can arise from free—free or recombination radiation. We feel that the most likely explanation for this extended emission is that it is an infrared reflection nebulosity. The implications of this interpretation are discussed below; discussion of several alternative possibilities is deferred to the following subsection.

4.3.1 *Reflection nebulosity*

If the extended region near IRS9 is reflection nebulosity then the absence of radio emission and the smoothness of the spatial distribution are readily explicable. With the information currently available it is not possible to deduce a unique model for the region, and many different arrangements for the illuminating sources and reflecting dust are conceivable. It is unclear, for example, whether or not the region is lit by one or by several sources of radiation. Nevertheless, in order to demonstrate that the existence of an infrared reflection nebula as large and as bright as this region is at least plausible, a simple model in which the extended region is illuminated solely by infrared radiation from the vicinity of the source IRS9 will be examined. The fact that the [1.65]—[2.2] μm colour of the nebulosity becomes redder with increasing distance from IRS9, after initially becoming bluer (Fig. 4), is consistent with this suggestion. A similar effect occurs in visible reflection nebulae such as the Merope Nebula (Greenberg & Roark 1967) and is attributed to reddening of the light from the illuminating star which is transmitted, rather than scattered, by the inner regions of the nebula. For the model to work it is necessary that there is more extinction along our direct line of sight to IRS9 than there is along the entire path from IRS9 to the extended emission region to the Sun. The reason for this is that the total 2.2-μm emission, and especially, the 1.65-μm emission, seen from the extended region exceeds that from IRS9 itself. The existence of such extinction local to IRS9 is consistent with the phenomenological model for this object developed above.

It can be shown that the colour temperature of the source which illuminates the reflection nebulosity must be $\gtrsim 850$ K. At the bluest point in the nebula, the [1.65]—[2.2] μm colour index is ~ 1.1 mag. Under the reasonable assumption that the scattering cross-section varies no faster than the λ^{-4} dependence characteristic of Rayleigh scattering, the cross-section is no more than $(2.2/1.65)^4 = 3.2$ times greater than 1.65 μm than at 2.2 μm. Thus the [1.65]—[2.2] μm colour index of the illuminating source is no redder than 2.4 mag; this corresponds to a colour temperature of 850 K or greater.

The energetics of the system are consistent with the reflection nebula hypothesis; for example, an 850 K blackbody at the distance of NGC 7538 having a total luminosity of $6 \times 10^4 L_\odot$ would have a 2.2-μm flux at the Earth of ~ 30 Jy. By contrast, the observed

2.2-μm flux density from the nebulosity, 250 mJy, is about 1 per cent of this. In this example, the reflected flux can be produced if the central 850 K object illuminates the nebula over a solid angle of ~ 1 sr, and if about 10 per cent of the illuminating radiation is scattered. This is not implausible, given that the 1-mm observations indicate a large column density of dust in this region, and that the albedos of certain types of grains, such as pure silicates or water ice, can be very large at 2.2 μm (Wickramasinghe 1973). Therefore, it appears that the reflection nebula model can be made to work for this source.

It is important to note that if the energy distribution of the radiation received directly from IRS9 (Fig. 2) were dereddened to a [1.65]–[2.2] μm colour index of 2.4 mag or less, as is consistent with the limit derived above, then the inferred total luminosity of IRS9 would exceed the limit of $6 \times 10^4 L_\odot$ set by the far-infrared observations. This discrepancy suggests that the object is asymmetrical in the sense that the reflection nebula is illuminated by radiation from an object at a significantly higher temperature than the dust which radiates the energy received directly from IRS9 at these wavelengths.

Several of the points raised above indicate that there is a non-spherical distribution of dust in the vicinity of the luminosity source in IRS9. Asymmetrical geometries have also been invoked to help to account for the morphology of cometary and biconical nebulae (Cohen 1974; Ney *et al.* 1975). The morphology of the extended emission near IRS9 is similar to that of these objects, which are believed to be reflection nebulae by virtue of their high polarization at optical and infrared wavelengths (Shawl & Tarenghi 1976; Cohen & Kuhi 1977; Jones & Dyck 1978). In considering these and other models for IRS9 it should also be remembered that, under the reflection nebula hypothesis, the absence of spectral features from the scattered emission (Fig. 3) sets additional constraints on the properties of this object and the nature of the underlying energy source.

4.3.2 *Other origins for the extended 2.2-μm emission*

Two other mechanisms which could be responsible for the 2.2-μm emission are radiation from an extended star cluster and radiation from hot dust. The total 2.2-μm flux density from this region, excluding IRS9, is about 250 mJy, spread over some 50-arcsec diameter beam areas. The intrinsic [1.65]–[2.2] μm colour indices of even the latest normal stars are less than 0.3 mag (Lee 1970); therefore the red colour of the extended emission must be due to extinction under this hypothesis. Since a typical [1.65]–[2.2] μm colour index for this region is about 2.5 mag, the 2.2-μm extinction in this region is typically about 3 mag if the extended emission is radiation from normal stars (*cf.* Becklin *et al.* 1978). The dereddened 2.2-μm flux density is therefore about 4 Jy. For this radiation to arise from solar-type stars would require the unreasonably large number of $\sim 10^4$ such stars. The alternative hypothesis — emission from a smaller number of late-type giants or supergiants — is rendered unlikely by the spatial uniformity of the emission and by the fact that there is no indication in the energy distribution of point B (Fig. 3) of the 2.3-μm CO feature associated with supergiants of spectral type later than K5.

The problem with the hypothesis that the emission is due to hot dust is that the dust needs to be very hot ($T \gtrsim 450$ K) over an extended area to produce extended emission at 2.2 μm. Dust temperatures in extended molecular clouds are typically a factor of 10 lower than this. Dust temperatures in compact H II regions are generally ~ 100–250 K (Wynn-Williams & Becklin 1974), but some grains may sometimes reach much higher temperatures in small areas (Wynn-Williams *et al.* 1978; see also Section 3.5). In these cases the dust is exposed to extremely strong ultraviolet radiation fields, which appear to be absent from the region near IRS9. Thus if the extended emission arises from heated dust, it seems that there

must be a large number of local sources of heating. Since the 2.2-μm emission is smoothly distributed over some 50 beam areas, the hot dust hypothesis, like the star cluster hypothesis, requires an uncomfortably large number of stars in a small volume.

It would be very useful to study the polarization of the extended 2-μm emission, since a reflection nebulosity ought to be highly polarized. Detailed molecular emission studies of the NGC 7538(E) region would also provide useful information about the interaction of IRS9 with the surrounding interstellar material.

5 Discussion: NGC 7538(S) and the extended H ɪɪ region

5.1 NGC 7538(S)

This region is observed at 1 mm and in the far-infrared as a dense, cold extension about 80 arcsec south of the main emission peak around NGC 7538-IRS1. The far-infrared luminosity of the region is $2 \times 10^4 L_\odot$ but, in contrast to most other infrared sources in regions of star formation, it has no detectable emission at 10 or 20 μm. In this respect the source somewhat resembles ON-3 near K3-50 and W75S(OH) (Wynn-Williams *et al.* 1977; Thronson & Harper 1978; Rieke *et al.* 1973; Harvey, Campbell & Hoffmann 1977; WBN) in that the maser emission coincides with strong far-infrared and submillimetre continuum emission but with only very weak 10- to 20-μm radiation.

The absence of a 10- to 20-μm source in NGC 7538(S) is surprising for two reasons. First, a source of luminosity is needed to power the far-infrared emission and, secondly, there are both observational and theoretical reasons for expecting a 10- to 20-μm source coincident with a maser source (e.g. Wynn-Williams & Becklin 1974). The existence of a large column density of dust in the vicinity of NGC 7538(S) has already been established by the presence of bright 100-μm and 1-mm emission there, so the most likely explanation for the apparent absence of a 10- to 20-μm source is that there is a very large amount of extinction in front of it. In the case of ON-3, Wynn-Williams *et al.* (1977) estimated that the extinction to the source was equivalent to several hundred magnitudes of visual extinction, and it is probable that a similar number applies here as well.

The nature of the faint extended emission at 2.2 μm near NGC 7538(S) is unknown. A possible explanation is that, like the extended emission near NGC 7538(E), it is a reflection nebulosity, illuminated either by IRS11 or by a hidden object.

5.2 THE OPTICAL H ɪɪ REGION

The present observations in the 25- to 130-μm waveband are of sufficiently high resolution that the emission from the diffuse, extended H ɪɪ region associated with the optical nebulosity may be separated from that arising from the nearby regions NGC 7538(N) and 7538(E). It is therefore possible to examine the energetics of the extended H ɪɪ region alone by comparing its radio and infrared emission. Israel's (1977) value of 19 Jy for the 5-GHz flux density may be used to calculate that the stars which ionize the nebula must produce $\sim 2 \times 10^{49}$ ionizing photon/s. If the ionizing stars are of type O8 or earlier, this implies that their total optical and ultraviolet luminosity is $\sim 2.5 \times 10^5 L_\odot$ (Panagia 1973). The measured 25- to 130-μm luminosity is $\sim 10^5 L_\odot$ (Table 1) so that even when allowance is made for emission at $\lambda < 25$ μm it would appear that the stars which ionize the gas can provide sufficient power to heat the dust in and around the H ɪɪ region. Two O stars which have been identified in the H ɪɪ region (Israel 1977) are marked as sources 5 and 6 in Plate 1(b). Their spectral types indicate they are sufficiently luminous to account for the radio and infrared fluxes.

At all three far-infrared wavelengths, the surface brightness of the emission from the optical H II region is highest to the south and south-east of the exciting stars; Plate 1 shows that this section of the source is the brightest at radio and optical wavelengths as well. The 100-μm maximum coincides with a region which appears as a bright rim on the radio map. It seems possible, therefore, that the 100-μm emission comes predominantly from dust just exterior to an ionization front, while the 30- and 50-μm emission is more associated with the dust within the H II region. The neutral material into which the H II region is expanding cannot have a large column density, however, since it is not prominent on the 1-mm map (Fig. 1(d)).

6 Star formation in NGC 7538

The NGC 7538 region shows a remarkable range of young objects in a small region of space. As well as several O stars in a diffuse H II region, it contains a group of three compact H II regions, two quite separate regions of OH/H$_2$O maser activity, two objects, IRS1 and IRS9, which look like infrared protostars, and a region of infrared reflection nebulosity. A molecular cloud seen at 1-mm wavelength embraces all the above except for the diffuse H II region and its associated stars.

There appears to be a large variety in the ages of the objects, in that the visible H II region has had time to dispel any obscuring matter which surrounded it, while the remainder of the objects remain hidden within the molecular cloud. Whether there is a variety in ages between the compact objects associated with the molecular cloud is less certain, though the possibility is certainly attractive that the sources IRS9-IRS1-IRS2-diffuse optical H II region represent an evolutionary sequence from infrared protostar, through ultracompact H II region plus maser, to compact H II region, to evolved H II region. It is interesting that this is a sequence in space as well as, perhaps, in time. It would appear that the centre of star formation is moving south-eastwards with time in this region.

Recent theoretical speculations (e.g. Elmegreen & Lada 1977) have centred on the idea that star formation is propagated in a spatial sequence of this type because the dynamical effects of each group of newly formed stars compress the adjacent neutral material and trigger its collapse. In the NGC 7538 region, the location of IRS1, IRS2, IRS3 and the southern maser sources in a dense cloud right at the edge of the diffuse H II region suggests that their collapse may have been triggered in this way (Israel 1977). In the case of IRS9, however, the evidence for such a direct dynamical interaction produced either by the diffuse H II region or by the compact H II regions is much less compelling.

7 Conclusions

(1) Far-infrared emission has been detected from four spatially separate regions within a total area some 5 pc in extent around NGC 7538. It is noteworthy that although these four regions have grossly similar properties in the far-infrared, each is heated by a group of stars or other compact luminosity sources of rather different characteristics. The total far-infrared luminosity of the NGC 7538 region is $\sim 5 \times 10^5 L_\odot$. Roughly one-half of this is attributable to the IRS1/IRS2/IRS3 cluster of compact dust-embedded H II regions, while the other half is due primarily to the stars which excite the optical nebula and to the newly discovered far-infrared source, NGC 7538(E).

(2) The newly discovered far-infrared source NGC 7538(E) is powered by a compact object, IRS9, whose infrared properties strongly resemble those of IRS1. The luminosity of IRS9 is $\gtrsim 6 \times 10^4 L_\odot$. A 40-arcsec diameter region of extended 2.2-μm emission near IRS9

appears to be an infrared reflection nebula illuminated by IRS9. Measurements of the polarization of this emission would provide a very useful test of this hypothesis. The apparent isolation of IRS9 from other significant luminosity sources, together with the diagnostic opportunities afforded by the reflection nebulosity, make this a good object against which models of dust-embedded young and forming stars can be tested.

(3) Observations in the 1-mm continuum show that a dense molecular cloud $\sim 2\,\mathrm{pc}$ in size, with a mass of $\sim 9 \times 10^3 M_\odot$, is located at the edge of the optical nebula and surrounds the compact H II regions IRS1/IRS2/IRS3, the southern maser sources and NGC 7538-IRS9. Infrared emission from the vicinity of the southern maser sources is seen at $100\,\mu\mathrm{m}$ but not at $10\,\mu\mathrm{m}$. The maser sources are therefore probably very deeply embedded within the molecular cloud.

(4) The far-infrared sources seen in the NGC 7538 region are powered by objects which range in evolutionary status from main sequence O stars to possible protostellar objects. The relative location of these objects suggests that the centre of star formation has moved with time systematically to the south-east in this region.

References

Allen, D. A. & Penston, M. V., 1974. *Nature*, **251**, 110.
Baldwin, J. R., Frogel, J. A. & Persson, S. E., 1973. *Astrophys. J.*, **184**, 427.
Becklin, E. E., Matthews, K., Neugebauer, G. & Willner, S. P., 1978. *Astrophys. J.*, **220**, 831.
Beetz, M., Elsässer, H., Poulakos, C. & Weinberger, R., 1976. *Astr. Astrophys.*, **50**, 41.
Blair, G. N., Evans, N. J., Vanden Bout, P. A. & Peters, W. L., 1978. *Astrophys. J.*, **219**, 896.
Cameron, R. M., Bader, M. & Mobley, R. E., 1971. *Appl. Opt.*, **10**, 2011.
Cohen, M., 1974. *Publs astr. Soc. Pacif.*, **86**, 813.
Cohen, M. & Kuhi, L. V., 1977. *Astrophys. J.*, **213**, 79.
Dyck, H. M. & Simon, T., 1977. *Astrophys. J.*, **211**, 421.
Elias, J. H., Ennis, D. J., Gezari, D. Y., Hauser, M. G., Houck, J. R., Lo, K. Y., Matthews, K., Nadeau, D. Neugebauer, G., Werner, M. W. & Westbrook, W. E., 1978. *Astrophys. J.*, **220**, 25.
Elmegreen, B. G. & Lada, C. J., 1977. *Astrophys. J.*, **214**, 725.
Gatley, I., Becklin, E. E., Werner, M. W. & Wynn-Williams, C. G., 1977. *Astrophys. J.*, **216**, 277.
Genzel, R. & Downes, D., 1977. *Astr. Astrophys. Suppl.*, **30**, 145.
Greenberg, J. M. & Roark, T. P., 1967. *Astrophys. J.*, **147**, 917.
Gruber, G. M. & de Jager, G., 1976. *Astr. Astrophys.*, **50**, 313.
Harris, S. & Scott, P. F., 1976. *Mon. Not. R. astr. Soc.*, **175**, 371.
Harvey, P. M., Campbell, M. F. & Hoffmann, W. F., 1977. *Astrophys. J.*, **211**, 786.
Ingersoll, A. P., Münch, G., Neugebauer, G. & Orton, G. S., 1976. *Jupiter*, p. 197, ed. Gehrels, T. University of Arizona Press.
Israel, F. P., 1977. *Astr. Astrophys.*, **59**, 27.
Israel, F. P., Habing, H. J. & de Jong, T., 1973. *Astr. Astrophys.*, **27**, 143.

Johnson, H. L., 1968. In *Nebulae and Interstellar Matter*, p. 167, eds. Middlehurst, B. M. & Aller, L. M., University of Chicago Press.

Jones, T. J. & Dyck, H. M., 1978. *Astrophys. J.*, **220**, 159.

Lee, T. A., 1970. *Astrophys. J.*, **162**, 217.

Martin, A. H. M., 1973. *Mon. Not. R. astr. Soc.*, **163**, 141.

Ney, E. P., Merrill, K. M., Becklin, E. E., Neugebauer, G. & Wynn-Williams, C. G., 1975. *Astrophys. J.*, **198**, L129.

Panagia, N., 1973. *Astr. J.*, **78**, 929.

Rieke, G. H., Harper, D. A., Low, F. J. & Armstrong, K. R., 1973. *Astrophys. J.*, **183**, L67.

Ryle, M., 1972. *Nature*, **239**, 435.

Shawl, S. J. & Tarenghi, M., 1976. *Astrophys. J.*, **204**, L25.

Thronson, H. A., Gatley, I., Harper, D. A., Becklin, E. E., Loewenstein, R., Moseley, S. H., Neugebauer, G. & Wynn-Williams, C. G., 1975. *Bull. Am. astr. Soc.*, **7**, 530.

Thronson, H. A., Jr & Harper, D. A., 1979. *Astrophys. J.*, in press.

Werner, M. W., Becklin, E. E. & Neugebauer, G., 1977. *Science*, **197**, 723.

Westbrook, W. E., Werner, M. W., Elias, J. H., Gezari, D. Y., Hauser, M. G., Lo, K. Y. & Neugebauer, G., 1976. *Astrophys. J.*, **209**, 94.

Wickramasinghe, N. C., 1973. *Light Scattering Functions for Small Particles*, J. Wiley, London.

Willner, S. P., 1976. *Astrophys. J.*, **206**, 728.

Wynn-Williams, C. G. & Becklin, E. E., 1974. *Publs astr. Soc. Pacif.*, **86**, 5.

Wynn-Williams, C. G., Becklin, E. E., Matthews, K. & Neugebauer, G., 1978. *Mon. Not. R. astr. Soc.*, **183**, 237.

Wynn-Williams, C. G., Becklin, E. E., Matthews, K., Neugebauer, G. & Werner, M. W., 1977. *Mon. Not. R. astr. Soc.*, **179**, 255.

Wynn-Williams, C. G., Becklin, E. E. & Neugebauer, G., 1974a. *Astrophys. J.*, **187**, 473.

Wynn-Williams, C. G., Werner, M. W. & Wilson, W. J., 1974b. *Astrophys. J.*, **187**, 41.